Third-order optical susceptibility in short-period GaAs doping superlattices

Kent D. Choquette
Materials Science Program, University of Wisconsin, Madison, Wisconsin 53706

Leon McCaughan
Electrical and Computer Engineering Department, University of Wisconsin, Madison, Wisconsin 53706

D. K. Misemer
Basic Technologies/Corporate Research Laboratory, 3M Company, St. Paul, Minnesota 55144

(Received 20 February 1989; accepted for publication 19 July 1989)

We propose that short-period doping superlattices are suitable for the enhancement of a third-order susceptibility arising from free carriers in nonparabolic energy subbands. The inherent advantage lies in the ability to simply engineer the superlattice potential profile, yielding control of miniband energy dispersion. We consider short-period GaAs doping superlattices composed of uniformly doped donor and acceptor layers, and planar-doped *n*- and *p*-type monolayers separated by intrinsic regions. Calculations of the electronic structure of compensated and *n*-type noncompensated *n-i-p-i* superlattices incorporating miniband dispersion at nonzero temperature are reported. We show that small modulations of the superlattice potential lead to large subband nonparabolicities and we calculate a twentyfold improvement in the third-order susceptibility over bulk GaAs at room temperature, comparable to that predicted for GaAs/AlGaAs compositional superlattices.

I. INTRODUCTION

Semiconductor superlattices allow the development of materials with enhanced optical and electrical characteristics over those found in their bulk constituents. Current semiconductor superlattices are either a periodic sequence of thin layers of two different semiconductors (compositional superlattice), or a periodic variation of impurities in an otherwise homogeneous semiconductor (doping or *n-i-p-i* superlattice). For both doping and compositional superlattices, a one-dimensional periodic potential is introduced in the direction of growth which modifies the bulk electronic band structure. Optical and electronic properties can therefore be engineered through selection of the superlattice fabrication parameters.

Doped bulk semiconductors, particularly small band-gap materials, exhibit nonresonant optical susceptibilities arising from the nonlinear motion of carriers in nonparabolic energy bands.[1] Such nonresonant optical nonlinearities would eliminate the necessity of light sources with well-defined wavelengths and avoid the large concomitant absorption inherent in resonant phenomenon (e.g., near-band-gap nonlinearities). That compositional semiconductor superlattices might also exhibit nonresonant optical nonlinearities has been recognized.[2-4] In a GaAs/AlGaAs superlattice with appropriate fabrication parameters, it has been calculated that electronic subband nonparabolicities should increase the third-order susceptibility, $\chi^{(3)}$, approximately 20–30 times over that found in bulk GaAs.[3,4]

An analogous optical nonlinearity will also be manifest in short-period doping superlattices.[5] We propose that the utilization of a doping superlattice is in fact more suitable for the enhancement of this $\chi^{(3)}$. The inherent advantage lies in the ability to simply design the profile of the space-charge-induced superlattice potential, modifying the subband energy dispersion and therefore miniband nonparabolicity. This $\chi^{(3)}$ is directly dependent upon both miniband nonparabolicity and free carrier density; to achieve an appreciable optical nonlinearity, doping superlattices with significant free carriers (i.e., noncompensated) must be considered. The electronic structure of a noncompensated *n-i-p-i* superlattice therefore requires a self-consistent solution,[6] unlike the straightforward calculation of a compensated doping superlattice.

This paper reports the theoretical investigation of short-period compensated and *n*-type noncompensated GaAs doping superlattices for optimization of a nonresonant third-order optical susceptibility. We consider two doping superlattice geometries: uniformly doped donor and acceptor layers, and planar-doped (δ-doped) *n*- and *p*-type monolayers separated by intrinsic regions. We first use compensated doping superlattice calculations to determine the potential profile which gives an optimum nonparabolic first subband, and then self-consistently determine the resulting optical nonlinearity in noncompensated doping superlattices possessing the same potential shape. In Sec. II the theory of $\chi^{(3)}$ due to electrons in nonparabolic minibands is described, and an expression for the thermally averaged subband nonparabolicity is derived. An outline of the calculation of electronic structure of doping superlattices taking into account subband dispersion at nonzero temperature is also included. The subband dispersion and resulting nonparabolicity found for compensated GaAs superlattices at room temperature is presented in Sec. III. In Sec. IV nonparabolic minibands are populated with electrons and the third-order susceptibilities in noncompensated doping superlattices are calculated. Section V is a discussion and summary of these results.

II. THEORY

Significant nonresonant optical susceptibilities are found in doped bulk semiconductors because of the nonlin-

 0021-8979/89/214387-06$02.40

ear motion of free carriers responding to driving optical fields.[1] Nonlinear motion of electrons arise in turn from a nonparabolic energy dispersion relationship. We consider the case of degenerate incident fields with polarization parallel to the superlattice growth direction. In analogy with bulk semiconductors,[7] the third-order susceptibility in the limit of long wavelength ($\hbar\omega \ll E_G$) for this situation is

$$\chi^{(3)}(\omega;\omega,\omega,-\omega) = [-ne^4/24(\hbar\omega)^4]\langle E^{(4)}\rangle, \qquad (1)$$

where electron concentration is n, and e is the charge of an electron. Other contributions to $\chi^{(3)}$ in this frequency degenerate case (such as electron energy dissipation via inelastic collisions[8]) which are not related to the superlattice properties are ignored. The thermally averaged nonparabolicity, $\langle E^{(4)}\rangle$, is given by

$$\langle E^{(4)}\rangle = \sum_{\mathbf{k}} f[E(\mathbf{k})]\frac{\partial^4 E}{\partial k_z^4} \Big/ \sum_{\mathbf{k}} f[E(\mathbf{k})], \qquad (2)$$

where $f[E]$ is the Fermi–Dirac distribution function. For n-doped bulk semiconductors using Kane's model[9] Eq. (2) becomes[1,4]

$$\langle E^{(4)}\rangle = \frac{6\hbar^4}{(m^*)^2 E_G}\left(\frac{1+8E_f/5E_G}{(1+4E_f/E_G)^{5/2}}\right), \qquad (3)$$

where m^* is the electron effective mass, E_G is the band-gap energy, and the Fermi energy E_f lies within the conduction band. For a semiconductor superlattice we use the effective mass approximation in directions transverse to the growth direction,

$$E(\mathbf{k}) = E_z(k_z) + E_t(k_t) = E_z(k_z) + (\hbar^2 k_t^2/2m^*), \qquad (4)$$

to obtain

$$\langle E^{(4)}\rangle = \frac{\int_0^{\pi/d} E_z^{(4)}\,dk_z \int_{E_z(k_z)}^{\infty} f[E_t]dE_t}{\int_0^{\pi/d} dk_z \int_{E_z(k_z)}^{\infty} f[E_t]dE_t} \qquad (5a)$$

which can be simplified[4] to give[10]

$$\langle E^{(4)}\rangle = \frac{-\int_0^{\pi/d} E_z^{(2)}\left(E_z^{(2)} f[E_z] + (E_z^{(1)})^2 \frac{\partial f}{\partial E}\right) dk_z}{\int_0^{\pi/d} k_z f[E_z] E_z^{(1)} dk_z + \frac{\pi}{d}\int_{E_z(\pi/d)}^{\infty} f[E_t]dE_t}, \qquad (5b)$$

where d is the superlattice period and $E^{(n)} \equiv (\partial/\partial k_z)^n E$. In Eqs. (5) only the first miniband is considered; a sum over subbands in Eqs. (5) would be required if higher subbands are occupied. Note that n in Eq. (1) corresponds to the electron density occupying the first miniband. In this paper derivatives are determined numerically, and hence the numerator of Eq. (5b) gives greater accuracy compared to Eq. (5a).

It is obvious from Eq. (2) that for this optical nonlinearity, dispersive subbands are required to achieve a finite contribution to $\chi^{(3)}$. The majority of the theoretical and experimental results from GaAs doping superlattices[11] corresponds to long-period geometries in which well-confined carriers occupy nondispersive energy levels in the growth direction. However, for short-period doping superlattices, wave functions of charge carriers in adjacent wells overlap sufficiently to give rise to dispersive subbands. As an example, the conduction minibands of a uniformly doped structure with its sinusoidal superlattice potential profile are sketched in Fig. 1. Equally spaced δ-doped monolayers separated by thin intrinsic regions result in a triangular potential profile (the so-called sawtooth n-i-p-i superlattice[12]). The superlattice potential barrier strongly affects the carrier wave function overlap between wells, and hence the potential profile will influence the miniband dispersion.

For compensated (or depleted) doping superlattices considered in Sec. III, the number of donors and acceptors are equal in each period ($n_D d_n = n_A d_p$), so the superlattice potential arises exclusively from the ionized impurities and can be determined analytically. For compensated superlattices the amplitude of the superlattice potential modulation will be[6]

$$V_{\max} = \frac{e^2}{\epsilon}\left[n_D\left(\frac{d_n}{2}\right)^2 + n_A\left(\frac{d_p}{2}\right)^2 + n_D d_n d_i\right], \qquad (6)$$

where ϵ is the dielectric constant and the fabrication parameters are uniform donor concentration n_D with layer thickness d_n, uniform acceptor concentration n_A with layer thickness d_p and intrinsic layer thicknesses of d_i. Notice that through judicious selection of superlattice parameters, a continuous variation of potential amplitude and periodicity ($d = d_n + d_p + 2d_i$) can be independently achieved.

For n-type noncompensated doping superlattices considered in Sec. IV ($n_D d_n > n_A d_p$), the superlattice potential arises from the contribution of both ionized impurities and free electrons. Thus, the superlattice potential, subband dispersion, and carrier distribution must be found self-consistently.[6] We utilize a procedure similar to that described by Zeller *et al.*,[13] extending the calculation to room temperature. The one-dimensional periodic potential is the combination of three terms[6]:

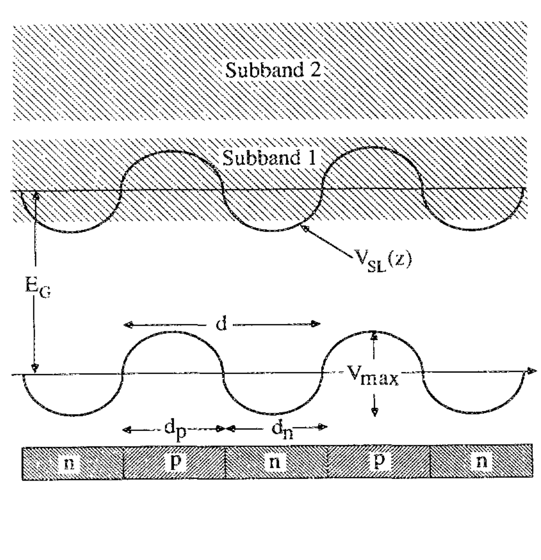

FIG. 1. Real space diagram of superlattice potential profile, $V_{SL}(z)$, conduction subbands (shaded regions), and dopant layer sequence of a uniformly doped short-period doping superlattice.

$$V_{\rm SL}(z) = \frac{e^2}{\epsilon}\int_0^z dz' \int_0^{z'} [n_A(z'') - n_D(z'')]dz'' + \frac{e^2}{\epsilon} \times \int_0^z dz' \int_0^{z'} [n(z'')]dz'' - 0.611\,\frac{e^2}{\epsilon}\left(\frac{3n(z)}{4\pi}\right)^{1/3}. \quad (7)$$

The first term represents the space-charge potential arising from bare ionized impurities found from integrating Poisson's equation. The second two terms, the Hartree, and the local exchange and correlation potential,[14] are dependent upon the electron distribution, $n(z)$.

Given a potential profile, the one-dimensional Schrodinger equation,

$$\frac{\hbar^2}{2m^*}\frac{d^2}{dz^2}\Psi_{ik_z} + [E_i(k_z) - V_{\rm SL}(z)]\Psi_{ik_z} = 0, \quad (8)$$

determines the eigenvalues, $E_i(k_z)$, and envelope wave functions, Ψ_{ik_z} (i is the subband index). The electron distribution is then given by

$$n(z) = \sum_i \frac{m^*}{\pi^2\hbar^2}\int_0^{\pi/d} |\Psi_{ik_z}|^2\, dk_z \int_0^{\infty} f[E_t + E_i(k_z)]dE_t. \quad (9)$$

The Fermi level is found from satisfying the condition

$$n = \sum_i \frac{m^*}{\pi^2\hbar^2}\int_0^{\pi/d} dk_z \int_0^{\infty} f[E_t + E_i(k_z)]dE_t, \quad (10)$$

where the total electron concentration in terms of the fabrication parameters is

$$n = (n_D d_n - n_A d_p)/d. \quad (11)$$

In our calculations we choose the upper limit of E_t in Eqs. (9) and (10) to be $E_f + 4k_BT$. The superlattice potential profile of n-type noncompensated superlattices are found by numerically solving Eqs. (7)–(10) utilizing an iterative self-consistent scheme. The criterion for self-consistency is that the relative root-mean-square variation of $n(z)$ is less than 10^{-6}, requiring typically four iterations.

With knowledge of the superlattice potential profile, $V_{\rm SL}(z)$, the subband dispersion of compensated and noncompensated doping superlattices are determined in detail numerically using the transfer matrix method.[15] The superlattice potential is approximated by division into 100 piecewise-constant elements. This scheme for determining the energy dispersion is based upon the continuity of the envelope wave functions and particle current density across the interfaces of the discretized potential. In the following sections the subband nonparabolicities of compensated and noncompensated GaAs doping superlattices are described.

III. COMPENSATED DOPING SUPERLATTICES

In Fig. 2 we plot $-\langle E^{(4)}\rangle$ vs period for δ-doped (solid curve) and uniformly doped (dashed curve) compensated GaAs doping superlattices at 300 K for two potential amplitudes. With the constraints of compensation and fixed potential magnitude, $V_{\max}$, each point of the dashed and solid curves correspond to specific values of dopant concentrations (see caption for descriptions of superlattices A, B, and C shown in Fig. 2). For comparison we also show the averaged nonparabolicity of rectangular potential profiles which

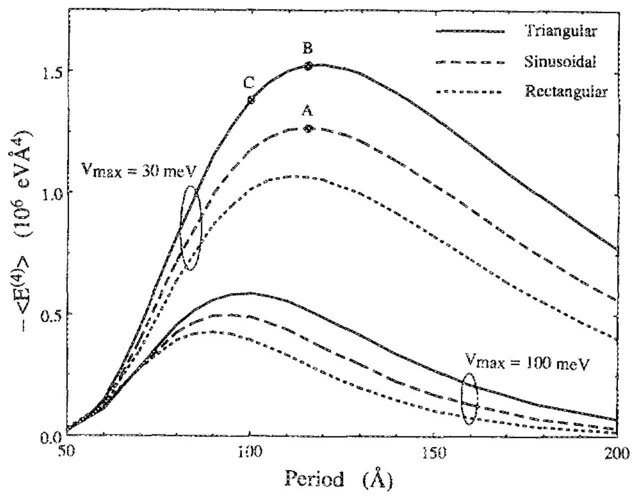

FIG. 2. Averaged first subband nonparabolicity vs period for GaAs compensated doping superlattices at 300 K for potential magnitudes of 30 and 100 meV. Superlattice potential profiles: triangular (planar doped); sinusoidal (uniformly doped); and rectangular (compositional superlattices). Fabrication parameters for superlattice A: $d_n = d_p = 57.5$ Å, $n_D = n_A = 2.6\times10^{18}$ cm^{-3}; superlattice B: $d_n = d_p = 2.5$ Å, $d_i = 55$ Å, $n_D = n_A = 3.0\times10^{19}$ cm^{-3}; superlattice C: $d_n = d_p = 2.5$ Å, $d_i = 47.5$ Å, $n_D = n_A = 3.5\times10^{19}$ cm^{-3}.

arise in compositional superlattice systems (dotted curve). A symmetric profile is assumed for all three potential shapes (triangular, sinusoidal, and rectangular) where the well widths equal the barrier widths. Uniformly doped superlattices with unequal dopant layer thicknesses ($d_n \neq d_p$) yield results which differ only slightly from Fig. 2. For the planar-doped superlattices we set $d_n = d_p = 2.5$ Å.

Notice in Fig. 2 the sign of the averaged nonparabolicity is negative, consistent with experimental measurements of $\chi^{(3)}$ for bulk GaAs.[16] The points of maximum $|\langle E^{(4)}\rangle|$ occur for periods of 90–120 Å. For shorter periods the magnitude of the averaged nonparabolicity is diminished as the subband dispersion approaches parabolic behavior; longer periods also exhibit less nonlinearity as the miniband gives way to an energy level. At a given period in Fig. 2, the magnitude of $\langle E^{(4)}\rangle$ increases as the superlattice potential amplitude decreases. Finally, note that for a given $V_{\max}$, planar-doped superlattices have larger subband nonparabolicities than uniformly doped structures, while the rectangular potential profiles produce the smallest values of the three.

Figure 3(a) illustrates the effect of different potential amplitudes on the superlattice energy dispersion relationship. As a specific example, we consider the first two subbands of two uniformly doped superlattices with identical layer thicknesses ($d = 115$ Å) and with potential magnitudes of 30 and 100 meV. A smaller $V_{\max}$ results in a narrower first miniband gap; as noted above, a smaller $V_{\max}$ also leads to greater subband nonparabolicity. This correlation between decreasing energy gap and increasing $\chi^{(3)}$ has been experimentally observed in bulk semiconductors[1] and has been predicted for compositional superlattices.[17] Plotted in Fig. 3(b) is the subband dispersion arising from the three

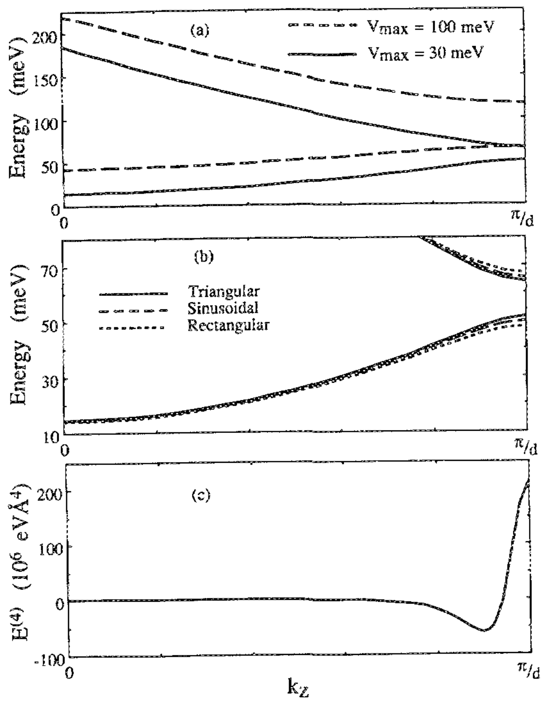

FIG. 3. Subband dispersion and fourth derivative of GaAs doping superlattices where $d = 115$ Å. Scale across mini-Brillouin zone given in units of π/d, and the zero of energy is the bottom of the wells. (a) Minibands of two uniformly doped superlattices with different superlattice potential amplitudes. (b) Subbands for the three superlattice potential profiles where $V_{\max} = 30$ meV. (c) Fourth derivative of first subband of uniformly doped superlattice A in Fig. 2.

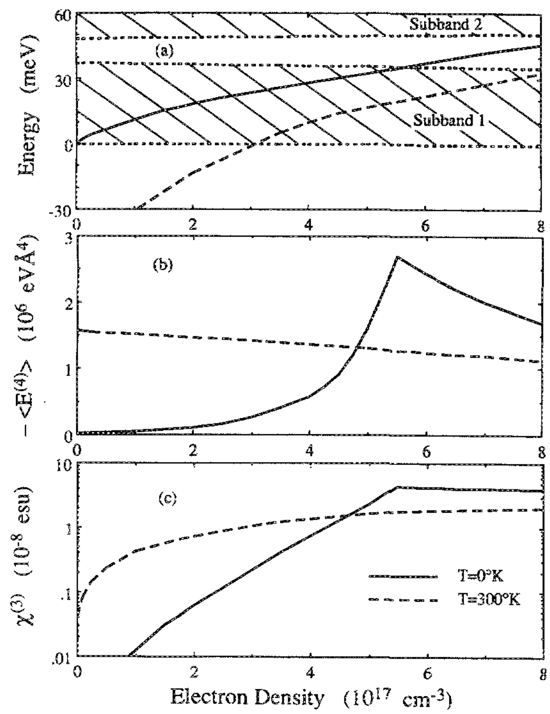

FIG. 4. Electronic and nonlinear properties vs total electron concentration, n, at zero and room temperature for uniformly doped noncompensated GaAs superlattices, where $d_n = d_p = 57.5$ Å, $n_A = 2.0 \times 10^{18}$ cm^{-3}, and $n_D = n_A + 2n$ cm^{-3}. (a) Fermi energy at $T = 0$ K (solid) and $T = 300$ K (dash); the hatched areas delineate the subband energies for both temperatures. (b) Averaged nonparabolicity at $T = 0$ K (solid) and $T = 300$ K (dash). (c) Third-order optical susceptibility at $\lambda = 10.6\,\mu$m for $T = 0$ K (solid) and $T = 300$ K (dash).

potential shapes for a common period of 115 Å and potential amplitude of 30 meV. The energies of the first subband for the triangular superlattice potential are above those of the sinusoidal potential profile, which in turn are greater than the first subband energies for the rectangular potential—the opposite trend holds for the second minibands. Comparing Figs. 2 and 3(b), the smallest first minigap possessed by the planer-doped superlattice corresponds again to the greatest first subband nonparabolicity. We show an example of $E^{(4)}$ vs k_z in Fig. 3(c) for superlattice A of Fig. 2. The maximum negative $E^{(4)}$ is found to occur near the upper edge (see also Ref. 4); however, for the highest states of the miniband, the fourth derivatives reverse sign. Therefore, an average over all occupied states of the subband is crucial in order to calculate the averaged nonparabolicity at nonzero temperatures.

We find the optimum nonlinearity will occur in doping superlattices with small potential amplitudes (e.g., 30 meV) and periods of 90–120 Å. Both planar and uniformly doped *n-i-p-i* geometries exhibit greater subband nonparabolicities than the compositional superlattice cases. The compensated sawtooth doping superlattice yields a maximum averaged subband nonparabolicity of -1.5×10^6 eV Å^4, a twentyfold improvement over undoped bulk GaAs at room temperature.

IV. NONCOMPENSATED DOPING SUPERLATTICES

The conduction miniband nonparabolicity treated in the previous section produces a third-order optical susceptibility upon introducing carriers into the subband. Shown in Fig. 4 are the electronic and nonlinear optical properties of uniformly doped noncompensated GaAs doping superlattices as a function of total electron concentration at absolute zero and room temperature. In these plots all superlattice parameters except donor concentration are held fixed; thus, as n_D increases, the excess electron population increases, and states of the first subband become occupied. The design parameters in this figure have been selected so that the noncompensated superlattice with the first miniband filled (at absolute zero) possesses the same potential amplitude ($V_{\max} = 30$ meV) and period ($d = 115$ Å) as the compensated superlattice A in Fig. 2.

The conduction subband edges and Fermi energy are shown in Fig. 4(a), where the zero of energy is the bulk GaAs conduction band edge. We find that the miniband energies calculated at 0 and 300 K vary negligibly. For these short-period superlattices the lowest subband energy is slightly lower than the bulk band edge, while the top of the first miniband extends above the superlattice potential maximum. At a donor concentration of $n_D = 3.1 \times 10^{18}$ cm^{-3} ($n = 5.5 \times 10^{17}$ cm^{-3}) the first subband is completely occupied at $T = 0$ K, and the potential profile and subband energies are nearly identical to those found in superlattice A in Fig. 2. Based on the results of Sec. III, an enhanced $|\langle E^{(4)}\rangle|$ and therefore $\chi^{(3)}$ is expected for this noncompensated superlattice.

At zero temperature the magnitude of the averaged nonparabolicity plotted in Fig. 4(b) initially increases as the states with subsequently larger fourth derivatives become occupied [see Fig. 3(c)]. As designed, the maximum $|\langle E^{(4)}\rangle|$ occurs at the electron concentration which just fills the first miniband. Beyond this carrier density the decreasing $-\langle E^{(4)}\rangle$ is a consequence of the increasing $V_{\max}$, similar to the behavior observed in Fig. 2. The third-order susceptibility at $T = 0$ K for $\lambda = 10.6\ \mu$m [Fig. 4(c), solid curve] approximately saturates when the first subband is filled: At electron densities greater than 5.5×10^{17} cm^{-3} the effect of increasing carrier concentration is nearly balanced by the decreasing $|\langle E^{(4)}\rangle|$. At room temperature, $-\langle E^{(4)}\rangle$ [Fig. 4(b), dashed curve] is smoothed out due to the influence of the higher thermally occupied miniband states. Hence, the room-temperature $\chi^{(3)}$ monotonically increases in Fig. 4(c) as a consequence of the increase in electron occupation of the subband, since the averaged nonparabolicity remains fairly constant.

Figure 5 is a comparison of the third-order susceptibility versus total electron concentration at room temperature and $\lambda = 10.6\ \mu$m for noncompensated planar and uniformly doped GaAs superlattices and bulk GaAs. For each superlattice curve the fabrication parameters except donor concentration are again held fixed. The structures A′, B′, and C′ indicated in Fig. 5 have a filled first subband (at $T = 0$ K) and the same potential profile as the compensated superlattices A, B, and C, respectively, of Fig. 2. [The third-order susceptibilities for the uniformly doped superlattices displayed in Fig. 4(c) are reproduced in Fig. 5.] The sawtooth noncompensated doping superlattices (solid and dotted curves) exhibit the greatest enhancement as expected.

The susceptibility can be further augmented by reducing the periodicity and increasing the carrier density. As an example, reducing the period of a planar-doped structure from 115 to 100 Å (superlattices B and C, respectively, in Fig. 2) and increasing the carrier concentration from 5.5×10^{17} to 7.5×10^{17} cm^{-3} (superlattices B′ and C′, respectively, in Fig. 5) gives a 25% increase in $\chi^{(3)}$. This occurs because a larger concentration of electrons can be accommodated in the first miniband of the shorter period superlattice which overcomes the reduction in the averaged nonparabolicity. Electron concentrations greater than 8×10^{17} cm^{-3} are not considered in Fig. 5 since significant occupation of the second miniband occurs, which is not accounted for in our calculations. The largest third-order susceptibility shown in Fig. 5 is 3.4×10^{-8} esu, which is a factor of 20 greater than the value for bulk GaAs, and corresponds to sawtooth doping superlattice with $d = 100$ Å, $n_D = 1.86\times10^{19}$ cm^{-3}, and $n_A = 1.7\times10^{19}$ cm^{-3}.

V. DISCUSSION

To achieve an improvement in the nonresonant $\chi^{(3)}$ in a semiconductor superlattice, Eq. (1) shows that a large density of carriers occupying nonparabolic subbands are desired. We have shown that for compensated GaAs doping superlattices, periods of 90–120 Å and small superlattice potential amplitudes lead to increased first miniband nonparabolicity. Furthermore, we find that n-type noncompensated superlattices with similar potential profiles exhibit the same nonparabolic subbands and are significantly populated at room temperature. Thus, we have shown both conditions can be fulfilled by proper choice of the design parameters of either δ-doped or uniformly doped GaAs n-i-p-i superlattices. The $\chi^{(3)}$ calculations reported in this paper have ignored the influence of the nonparabolicity of higher minibands, and any contribution to the optical nonlinearity due to intersubband transitions.

Reducing the potential barrier between the electron wells gives a narrower energy gap between the first and second minibands. Greater nonparabolicity in the first subband is then expected, in analogy with Kane model[9] of narrow band gap bulk semiconductors and the Kronig–Penny model[17] for compositional superlattices. The increase in the nonparabolicity with decreasing superlattice barrier will not continue indefinitely: In the limit of negligible superlattice potential, parabolic energy dispersion will be recovered with no contribution to the third-order susceptibility. [Notice the bulk nonparabolicity, Eq. (3), vanishes in the limit of small and large energy gaps.] Our calculations, however, predict that $|\langle E^{(4)}\rangle|$ monotonically increases as the potential amplitude decreases; we conservatively estimate that our numerical results are reliable for superlattice potential amplitudes greater than 10 meV.

Two important assumptions in our calculations of the space-charge-induced superlattice potential are that donor

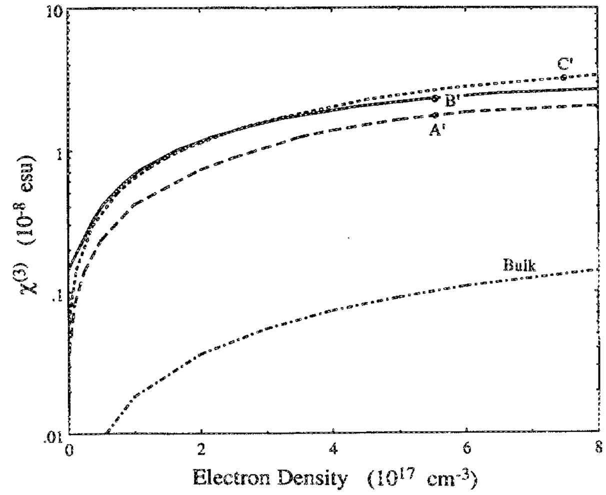

FIG. 5. Third-order susceptibility vs total electron concentration at $\lambda = 10.6\ \mu$m and room temperature for noncompensated GaAs doping superlattices and bulk GaAs (dot-dash). The fabrication parameters are $n_D = n_A + 2n$ cm^{-3} and: (i) planar-doped $d_n = d_p = 2.5$ Å, $d_i = 55$ Å, $n_A = 1.5\times10^{19}$ cm^{-3} (solid); (ii) planar-doped $d_n = d_p = 2.5$ Å, $d_i = 47.5$ Å, $n_A = 1.7\times10^{19}$ cm^{-3} (dotted); (iii) uniformly doped $d_n = d_p = 57.5$ Å, $n_A = 2\times10^{18}$ cm^{-3} (dashed). The superlattices A′, B′, and C′ possess the same potential profile and subband structure as superlattices A, B, and C, respectively, in Fig. 2.

impurity bands and spatial potential fluctuations arising from the random distribution of impurities can be ignored. Both of these aspects have been addressed in Ref. 6. Neglecting donor impurity bands in GaAs is valid due to the small effective electron mass and small binding energy of typical donors; hence, electrons can be expected to populate the superlattice conduction subbands and not impurity levels. The short-range potential fluctuations, arising from the random distribution of the dopants for the impurity densities considered, is estimated to be less than 30 meV as determined from the unscreened Coulomb energy of a point charge separated by an average distance from an ionized impurity. Notice that in noncompensated doping structures the screening by free electrons should further reduce the potential fluctuations. We have taken 30 meV to be the minimum realistic doping superlattice amplitude in uniformly doped structures possessing impurity concentrations on the order of 10^{18} cm^{-3}. Recently, it has been shown that sawtooth doping superlattices exhibit smaller potential fluctuations[18] and therefore smaller potential modulations and larger nonlinear enhancements may be possible in these materials.

The subband nonparabolicities and resulting third-order susceptibility in the GaAs/AlGaAs compositional superlattice system have been calculated in detail by Chang.[4] The author reports a GaAs/$Al_{0.1}Ga_{0.9}As$ superlattice with well thickness of 57 Å, barrier thickness of 14 Å, and a carrier concentration of 1.8×10^{18} cm^{-3} gives a third-order susceptibility which is 20 times higher than the value in bulk GaAs at room temperature. For GaAs noncompensated doping superlattices we also calculate a twentyfold improvement. Compared to the GaAs/AlGaAs system, we find the optimum GaAs doping superlattices have longer period lengths and require less electron densities, because of larger enhancements in the first subband nonparabolicity. Fabrication of the optimum noncompensated doping superlattices described in Sec. IV is feasible, for example, by molecular-beam epitaxy. The third-order susceptibility of uniformly doped and δ-doped structures are equivalent as compared to bulk GaAs. However, due to reduced potential fluctuations and the demonstrated feasibility of growth, sawtooth GaAs *n-i-p-i* superlattices may prove to be superior materials for nonresonant $\chi^{(3)}$ enhancements.

[1] C. K. N. Patel, R. E. Slusher, and P. A. Fleury, Phys. Rev. Lett. **17**, 1011 (1966); P. A. Wolff and G. A. Pearson, Phys. Rev. Lett. **17**, 1015 (1966).
[2] R. Tsu and L. Esaki, Appl. Phys. Lett. **19**, 246 (1971).
[3] W. Bloss and L. Friedman, Appl. Phys. Lett. **41**, 1044 (1982); G. Cooperman, L. Friedman, and W. Bloss, Appl. Phys. Lett. **44**, 977 (1984).
[4] Y. Chang, J. Appl. Phys. **58**, 499 (1985).
[5] K.D. Choquette and L. McCaughan, *Topical Meeting on Optical Properties of Materials, 1988 Technical Digest Series* (Optical Society of America, Washington, DC, 1988), Vol. 9, pp. 49.
[6] P. Ruden and G. Dohler, Phys. Rev. B **27**, 3538 (1983).
[7] S. Jha and N. Bloembergen, Phys. Rev. **171**, 891 (1968).
[8] S. Y. Yuen and P. A. Wolff, Appl. Phys. Lett. **40**, 457 (1982).
[9] E. O. Kane, J. Phys. Chem. Solids **1**, 249 (1957).
[10] After integration-by-parts of Eq. (5a), we find an additional boundary-term integral in the denominator of Eq. (5b) which is not present in Eq. (19) of Ref. 4.
[11] G. Dohler, in *Synthetic Modulated Structures*, edited by L. Chang and B. Giessen (Academic, New York, 1985).
[12] E. F. Schubert, Y. Horikoshi, and K. Ploog, Phys. Rev. B **32**, 1085 (1985); E. F. Schubert, J. E. Cunningham, and W. T. Tsang, Phys. Rev. B **36**, 1348 (1987).
[13] Ch. Zeller, B. Vinter, and G. Abstreiter, Phys. Rev. B **26**, 2124 (1982).
[14] W. Kohn and L. Sham, Phys. Rev. **140**, A1133 (1965).
[15] V.Tripathi and P. Bhattacharya, Superlattices and Microstructures **1**, 73 (1985).
[16] J. Wynne, Phys. Rev. **178**, 1295 (1969).
[17] C. M. de Sterke and D. G. Hall, Appl. Phys. Lett. **47**, 1260 (1985).
[18] E. F. Schubert, T. D. Harris, and J. E. Cunningham, Appl. Phys. Lett. **53**, 2208 (1988).